VORTEX-INDUCED VIBRATIONS USING WAKE OSCILLATOR MODEL COMPARISON ON 2D RESPONSE WITH EXPERIMENTS

David Cébron
Ecole Centrale Nantes, Nantes, France
Benoît Gaurier & Grégory Germain
IFREMER, Hydrodynamics and Metocean, 62 200 Boulogne-sur-Mer, France

ABSTRACT

A model using wake oscillators is developed to predict the 2D motion in a transverse plan of a rigid cylinder in a flow. This model of the wake dynamics is validated on a single cylinder for which we consider both transverse and in-line response. The good agreement between the model and the experimental results allows to use this model as a simple computation tool in the prediction of 2D Vortex-Induced Vibrations (VIV) and after futher development Wake-Induced Oscillations (WIO) effects.

1. INTRODUCTION

Mooring and flow lines involved in offshore systems for oil production are submitted to various solicitations. Among them the effects of current are dominating. Vortex-Induced Vibrations (VIV) and Wake-Induced Oscillations (WIO) on closely spaced marine risers may lead to fatigue, clashes and structural failures. Extended studies have been conduced to describe and explain them for spring mounted uniform cylinders in translation perpendicularly to their main axis (Sarpkaya, 2004). In the case of a pivoted cylinder with uniform diameter (Flemming and Williamson, 2005) a similar response is observed with some variations on the reduced velocity interval and maximum response.

Experiments on model scaled tests with real configurations for dual risers interaction in a uniform current were performed in the Ifremer flume tank, within the framework of the project Clarom CEPM CO 3007/04 in partnership with Doris engineering, Saipem S.A., Institut Français du Pétrole, Océanide, Ecole Centrale Marseille and Total. The behaviour of two risers exposed to steady current and excited by VIV and WIO were studied (Germain et al, 2006). These tests give a lot of information on how fluid interaction between two cylinders of equal diameter in tandem configuration can significantly modify their structural response in term of amplitude and frequency, compared to a single one (Gaurier et al, 2007a). Both in-line and cross-flow response have been studied and presented as functions of the reduced velocity. Results demonstrate that wake effects can be relatively strong. In almost all the tested cases the upstream cylinder responds like an isolated single one, whereas the vortex shedding and synchronization of the downstream cylinder can be strongly affected by the wake of the upstream one. Those phenomenons are relatively hard to predict.

In order to quantify those wake effects, we developed a 2D phenomenological model of the near wake based on Van Der Pol wake oscillator (Facchinetti, 2004 and Violette et al, 2007) which describes the 2D motion of the cylinder in its transverse plan. This simplified model of the wake dynamics is here validated on a single cylinder for which we consider the 2D response. The model will be extended for the case of two cylinders in interaction in a future work.

2. MATHEMATICAL MODEL

2.1. Dynamic equations in 2D

Initially, dynamic equations are only written for a single cylinder in transverse motion and have been generalised for a cylinder in free motion in its transverse plan. For an oscillating cylinder (mass m, volume V, velocity $\overrightarrow{\dot{X}}$) submit to a current described by: $\overrightarrow{U} = U_x(t)\ \overrightarrow{e_x} + U_y(t)\ \overrightarrow{e_y}$, we can write:

$$m\ \overrightarrow{a_r} = \sum \overrightarrow{F_{ext}} + \overrightarrow{f_{ie}} + \overrightarrow{f_{ic}} \qquad (1)$$

with $\overrightarrow{a_r} = \overrightarrow{\ddot{X}} - \overrightarrow{\dot{U}}$ the relative acceleration, $\overrightarrow{f_{ie}} = -m\ \overrightarrow{\dot{U}}$ the inertial force and $\overrightarrow{f_{ic}} = \overrightarrow{0}$ the Coriolis force.

The exterior forces $\sum \overrightarrow{F_{ext}}$ contain the hydrodynamic forces, the spring force and possibly structural damping forces:

$$\sum \overrightarrow{F_{ext}} = \overrightarrow{F_{hydro}} + \overrightarrow{f_{spring}} + \overrightarrow{f_{damping}} \quad (2)$$

with:

$$\overrightarrow{F_{hydro}} = \underbrace{\overrightarrow{F_D}}_{drag} + \underbrace{\overrightarrow{F_L}}_{lift} + \underbrace{\rho V \dot{\overrightarrow{U}} - C_m \rho V \overrightarrow{a_r}}_{potential\ theory} \quad (3)$$

$$\overrightarrow{F_D} = -\frac{1}{2}\rho S C_D \|\dot{\overrightarrow{X}} - \overrightarrow{U}\|(\dot{\overrightarrow{X}} - \overrightarrow{U}) \quad (4)$$

$$\overrightarrow{F_L} = -\frac{1}{2}\rho S C_L \|\dot{\overrightarrow{X}} - \overrightarrow{U}\|(\dot{\overrightarrow{X}} - \overrightarrow{U})^{\perp} \quad (5)$$

$$\overrightarrow{f_{spring}} = -k\left(\overrightarrow{X} - \overrightarrow{X_0}\right) \quad (6)$$

$$\overrightarrow{f_{damping}} = -\lambda \dot{\overrightarrow{X}} \quad (7)$$

and ρ the mass density, C_m the added mass coefficient, C_D the drag coefficient, C_L the lift coefficient, k the stiffness and λ the linear structural damping.

In projection, with $\overrightarrow{F_L} = \overrightarrow{e_z} \times \overrightarrow{F_D}$, we obtain:

$$\begin{cases} (m + C_m\rho V)\ddot{x} + \lambda\dot{x} + k(x - x_0) = \\ \frac{1}{2}\rho S\left[C_D(U_x - \dot{x}) - C_L(U_y - \dot{y})\right] \times \\ \sqrt{(U_x - \dot{x})^2 + (U_y - \dot{y})^2} + \rho V(1 + C_m)\dot{U_x} \\ \\ (m + C_m\rho V)\ddot{y} + \lambda\dot{y} + k(y - y_0) = \\ \frac{1}{2}\rho S\left[C_D(U_y - \dot{y}) + C_L(U_x - \dot{x})\right] \times \\ \sqrt{(U_x - \dot{x})^2 + (U_y - \dot{y})^2} + \rho V(1 + C_m)\dot{U_y} \end{cases} \quad (8)$$

We can notice that without lift, this last equation is the generalized formula of Morison (Morison et al, 1950).

Those previous forces are those in laminar flow, without vortex. But in turbulent flow, we have to add:

1. *fluctuating forces* created by vortex which can be written in this generally decomposition:

$$\overrightarrow{F_{Df}} = -\frac{1}{2}\rho S C_{Df} \|\dot{\overrightarrow{X}} - \overrightarrow{U}\|(\dot{\overrightarrow{X}} - \overrightarrow{U}) \quad (9)$$

$$\overrightarrow{F_{Lf}} = -\frac{1}{2}\rho S C_{Lf} \|\dot{\overrightarrow{X}} - \overrightarrow{U}\|(\dot{\overrightarrow{X}} - \overrightarrow{U})^{\perp} \quad (10)$$

Expressions of C_{Df} and C_{Lf} depend of the model. In a first rough model, these coefficients are often approximated by sinusoidal functions.

2. *blockage drag* which is the additional drag issued from the transverse motion of the cylinder: this motion increases the apparent projected surface in front of the flow. We cannot just adjust the drag coefficient by a factor because a rise of the relative longitudinal velocity of the flow increases the steady drag but does not increase the blockage drag. So we can write, with a usual form:

$$\overrightarrow{F_{Db}} = \frac{1}{2}\rho S C_{Db} \sqrt{U_x^2 + U_y^2} \begin{bmatrix} U_x \\ U_y \end{bmatrix} \quad (11)$$

Skop et al (1977) propose an empirical expression for this coefficient:

$$C_{Db} = 1.16 C_D \left[\left(1 + 2\frac{A}{D}\right)\frac{f_{ex}}{f_{st}} - 1\right]^{0.65} \quad (12)$$

where f_{ex} is the frequency of transverse oscillation, f_{st} is the vortex shedding frequency, issued from the Strouhal number, and A is the amplitude of the transverse motion.

Finally, we can write the final general equations:

$$\begin{cases} (m + C_m\rho V)\ddot{x} + \lambda\dot{x} + k(x - x_0) = \\ \frac{1}{2}\rho S\left[(C_D + C_{Df})(U_x - \dot{x}) - (C_L + C_{Lf})(U_y - \dot{y})\right] \times \\ \sqrt{(U_x - \dot{x})^2 + (U_y - \dot{y})^2} + \rho V(1 + C_m)\dot{U_x} + \\ \frac{1}{2}\rho S C_{Db}\sqrt{U_x^2 + U_y^2}\, U_x \\ \\ (m + C_m\rho V)\ddot{y} + \lambda\dot{y} + k(y - y_0) = \\ \frac{1}{2}\rho S\left[(C_D + C_{Df})(U_y - \dot{y}) + (C_L + C_{Lf})(U_x - \dot{x})\right] \times \\ \sqrt{(U_x - \dot{x})^2 + (U_y - \dot{y})^2} + \rho V(1 + C_m)\dot{U_y} + \\ \frac{1}{2}\rho S C_{Db}\sqrt{U_x^2 + U_y^2}\, U_y \end{cases} \quad (13)$$

2.2. Vortex forces

Following Facchinetti et al (2004), the vortex forces could be modeled by Van Der Pol oscillators coupled with the acceleration of the cylinder:

$$\begin{cases} \ddot{C}_{Df} + \varepsilon_D \, 2\omega_{st} \left(\left(\dfrac{2\, C_{Df}}{C_{Df_0}} \right)^2 - 1 \right) \dot{C}_{Df} \\ + (2\omega_{C_L})^2 \, C_{Df} = A_D(\ddot{x} - \dot{U}_x) \\ \ddot{C}_{Lf} + \varepsilon_L \, \omega_{st} \left(\left(\dfrac{2\, C_{Lf}}{C_{Lf_0}} \right)^2 - 1 \right) \dot{C}_{Lf} \\ + \omega_{C_L}^2 \, C_{Lf} = A_L(\ddot{y} - \dot{U}_y) \end{cases} \tag{14}$$

where C_{Df_0} and C_{Lf_0} are the amplitudes of the fluctuating drag and lift coefficients, ω_{st} is the vortex shedding pulsation, issued from the Strouhal number. Facchinetti et al (2004) and Violette et al (2007) use $A_L = 12$ and $\varepsilon_L = 0.3$ for 1D motion, while we use here: $A_L = A_D = 10$, $\varepsilon_D = 1.2$ and $\varepsilon_L = 2.5$.

2.3. Analytic studies of data

For the accuracy of the model, the evolution of hydrodynamical coefficients must be known precisely. So, bibliographical data from Sarpkaya (1978), Sarpkaya (2004), Schlichting (1951), Norberg (2001) and Cantwell and Coles (1983) are fitted to obtain analytic formulas, versus Reynolds number $Re = UD/\nu$ or reduced velocity $V_r = U/(f_{com}D)$.

2.3.1. Drag coefficient

For $Re = 0.1$ to $Re = 10^5$, we can approximate C_D (15%) by:

$$\log C_D = 1.0444 \log \frac{Re^{0.246}}{10} \log \frac{Re^{0.318}}{10} \tag{15}$$

For $Re = 10^5$ to $Re = 4.10^5$, C_D is experimentally known:

$$C_D = 1.2 \tag{16}$$

For $Re = 4.10^5$ to $Re = 8.10^6$, we can approximate C_D (20%) by:

$$C_D = 0.6 + \left[\frac{0.873}{\log(Re) - 4.7} \right]^{12} - \left[\frac{0.873}{\log(Re) - 4.7} \right]^{2.923} \tag{17}$$

2.3.2. Strouhal number

For $Re = 50 - 10^7$, we can approximate St (1.5%) by:

$$St = 0.257 \log \frac{Re^{0.175}}{100} \log \frac{Re^{0.891}}{10} \times \left[\log \frac{Re^{0.309}}{10} - \log^2 Re^{0.172} \right] \tag{18}$$

2.3.3. Added mass

For $V_r < 4.5$, we can approximate C_m (5%) by:

$$C_m = 77.2 \; 10^{-3} \; V_r^2 - 0.133 \; V_r + 1.03 \tag{19}$$

For $V_r \geq 4.5$, we can approximate C_m (35%) by:

$$C_m = 15250 \; e^{-2V_r} - 1.618 \left(\frac{A}{D} \right)^2 + 2.471 \left(\frac{A}{D} \right) - 1.532 \tag{20}$$

If we consider the natural frequency f_{com} of the system equal to the frequency of the vortex shedding f_{st} for the range of reduced velocity of lock-in:

$$f_{com} = \frac{1}{2\pi} \sqrt{\frac{k}{m + C_m \rho V}} = f_{st} = \frac{S_t U}{D} \tag{21}$$

we can refine the value of the added mass in the lock-in region:

$$C_m = \frac{1}{\rho V} \left[\frac{k}{(2\pi S_t f_{com} V_r)^2} - m \right] \tag{22}$$

This expression is connected with 19 and 20 at the vertices.

2.3.4. Correlation length

Experiments show that, for turbulent shedding flows, the vortex shedding does not occur in phase over the whole span. Thus, the correlation between two sectional fluctuating forces separated by a certain spanwise distance s, decreases when s increase (Norberg, 2002). Assuming spanwise homogeneity, the ratio γ_L between the r.m.s. lift on a finite length l and the sectional r.m.s. lift times l is (Kracker et al, 1974):

$$\gamma_L = \frac{1}{l} \sqrt{2 \int_0^l (l - s) R_{LL}(s) \, ds} \tag{23}$$

with:

$$R_{LL}(s) = \frac{\overline{F_{L_{s1}} \, F_{L_{s2}}}}{\sqrt{\overline{F_{L_{s1}}^2}} \sqrt{\overline{F_{L_{s2}}^2}}} = \frac{\overline{F_{L_{s1}} \, F_{L_{s2}}}}{F_{L_{RMS \; s1}} F_{L_{RMS \; s2}}} \tag{24}$$

which is the Pearson's correlation coefficient between the lift on the section $s1$ of the cylinder and the lift of the section $s2$.

The correlation length is defined by Norberg (2002):

$$\Lambda_L = \int_0^\infty R_{LL}(s) \, ds \tag{25}$$

And experimental data show that it is possible to write:

$$R_{LL}(s) = e^{-\frac{s}{\Lambda_L}} \tag{26}$$

So we deduce:

$$\gamma_L = \frac{\sqrt{2}}{l/\Lambda_L}\sqrt{e^{-l/\Lambda_L} + l/\Lambda_L - 1} \tag{27}$$

γ_L is calculated from equations supplied in Norberg (2002) which give the ratio Λ_L/D and so, we can calculate the lift on the entire cylinder with the sectional r.m.s. lift $F_{L_{RMS}}$. If we note $C_{L_{RMS}}$ the sectional r.m.s. lift coefficient given in Norberg (2002), we have:

$$F_{L_{RMS}} = \frac{1}{2}\rho S C_{L_{RMS}} U^2 \tag{28}$$

2.4. Link with experimental data

To compare this model with our experimental data (Gaurier et al, 2007a), we have to link it to a pendulum motion of a rigid cylinder elastically mounted in a flow. Considering little angles, we can transform the pendulum equations in linear translation equations. To do this, we have to use, in the linear equation, the mass and the stiffness linked with the slice of the cylinder considered and located at $z = 1.348\ m$. We use:

$$m = \frac{I}{z^2} \quad \text{and} \quad k = \frac{K}{z^2} \tag{29}$$

with I the moment of inertia, K the angular stiffness and m the equivalent mass and k the equivalent stiffness.

We use a structural damping coefficient $\zeta = 1\%$ in agreement with experimental free decay test in calm water.

2.5. Algorithm

The numerical scheme used to solve this problem is the implicit numerical differentiation formulas `ode15s` of orders 1 to 5, from Matlab and especially designed for stiff systems (Ashino et al, 2000).

To solve equations 13 and 14, we need also to know C_{Db} and C_m, which are dependant of the amplitude A and of the frequency of transverse oscillation f_{ex}. To solve this dependency problem, the algorithm used makes iterative loops while $C_{Db_{i+1}} - C_{Db_i}$ and $C_{m_{i+1}} - C_{m_i}$ is greater than a certain value, fixed here at 0.01. Then, when C_{Db} and C_m are converged, the stream velocity is incremented and the motion achieved.

3. COMPARISON WITH EXPERIMENTS

3.1. Free decay test

A free decay test is a good way to check the natural frequency calculated and to give a first validation of the model. Equations 14 are written for relative flow velocity. So, we can used it to predict a free decay test in calm water. To do this, we define a characteristic velocity of the cylinder v_c to calculate a Reynolds number different from zero:

$$Re_g = \frac{D|U - v_c|}{\nu} = \frac{D}{\nu}\left|U - f_{com}\sqrt{x_0^2 + y_0^2}\right| \tag{30}$$

with f_{com} the natural frequency in water and (x_0, y_0) the initial position of the cylinder.

The figure 1 shows an excellent agreement for both frequency and amplitude between the model and the experimental results.

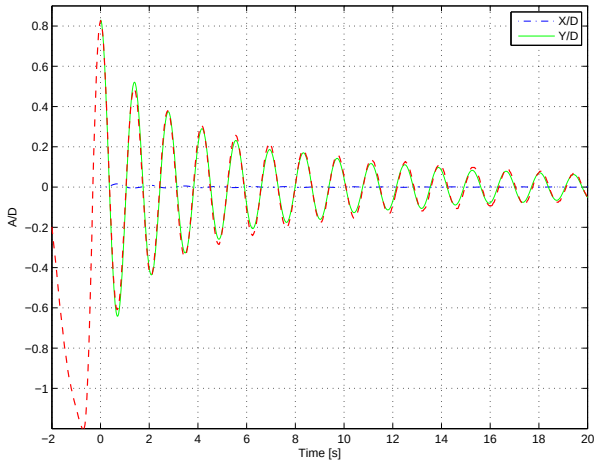

Figure 1: *Oscillations of the cylinder during a free decay test. Dash line: transverse displacement of the experimental cylinder, dash-dot line: in-line and solid line: transverse displacements of the cylinder of the model.*

The initial transverse position is 0.8 D. The mean hydrodynamical coefficients calculated by the model during this test are: $C_m = 0.98$, $S_t = 0.215$ and $C_{Db} = 0$. These values are agreed with the classical bibliographical results.

3.2. Free cylinder in a flow

To validate the model in a large range of reduced velocity, we can compare the complementary characteristics: mean and r.m.s. displacements between experiments and model.

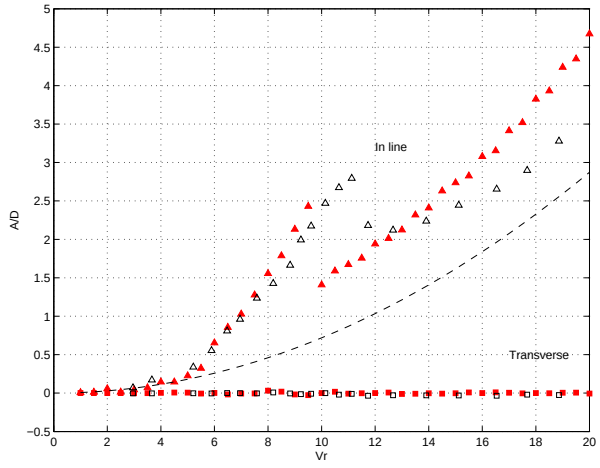

Figure 2: *Mean displacements of the cylinder. Transverse oscillations:* ▲ *model,* △ *experiments. In-line oscillations:* ■ *model,* □ *experiments. The dash line is the quasi-static result.*

On figure 2, the mean transverse displacement is of course null for all the reduced velocities, contrary to the mean in-line displacement, which is always increasing with the velocities. The change on slope at $V_r = 10$ comes from the end of the lock-in. This sudden gap arrives at a lower reduced velocity for the model (at $V_r = 10$) than for experiments (at $V_r = 11$).

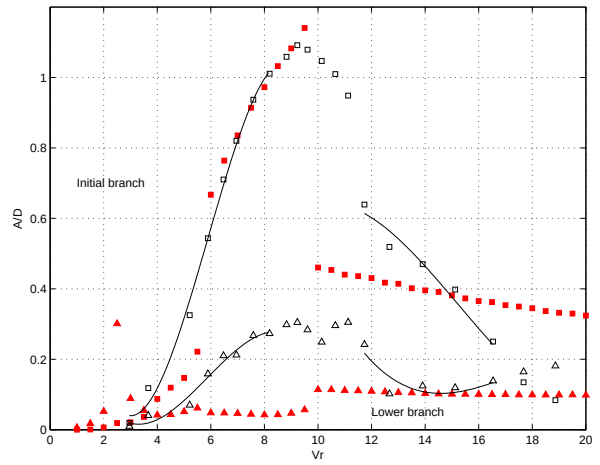

Figure 3: *Standard deviation of the displacements of the cylinder. Transverse oscillations:* ▲ *model,* △ *experiments. In-line oscillations:* ■ *model,* □ *experiments.*

On figure 3, the three branches introduced by Jauvtis and Williamson (2003) are plotted on the transverse displacements: the *initial branch* for $Vr < 6$, the *upper branch* for $6 \leq V_r < 10$ and the *lower branch* for $V_r \geq 10$. Comparing with the experimental data, the gap between the *upper branch* and the *lower branch* appears at $V_r = 10$ for the model, whereas it appear es at $V_r = 11$ experimentally. This difference comes from the instabilities observed during experiments for these velocities: the transition from the upper to lower branch involves an intermittent switching between two modes (Gaurier et al, 2007b).

Finally, in-line r.m.s. displacements seem to be less in agreement with the experimental data than the previous data. However, the comparison with bibliographical results like Jauvtis and Williamson (2004) shows that the model reproduce correctly the in-line r.m.s. displacements for $V_r < 4$, including the amplification of the motion at $1.7 < V_r < 2.3$ named the *second instability region* by Sarpkaya (2004). Model results are also in relative good agreement for $V_r > 10$. However, these displacements are not reproduced during the lock-in. The origin of this difference comes from the amplification of the amplitude of C_{Df_0} which is not take into account here. Indeed, contrary to the amplitude of the fluctuating lift coefficient C_{Lf_0}, no bibliographical data were found on this subject. So, this coefficient is considered constant in the model.

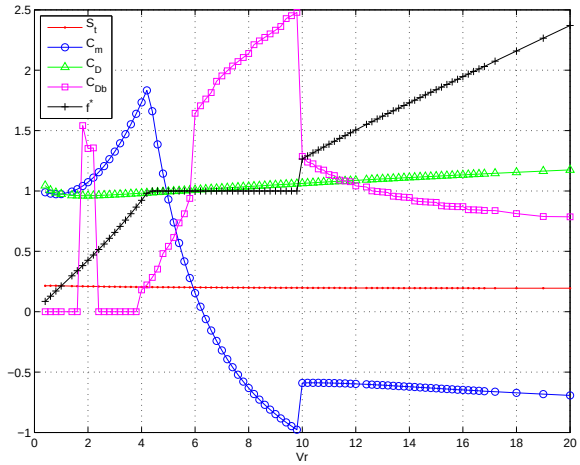

Figure 4: *Hydrodynamical coefficients versus reduced velocity.* ●*: Strouhal number,* ○*: added mass coefficient,* △*: drag coefficient,* □*: blockage drag coefficient and* +*: reduced frequency.*

It is also interesting to check the evolution of the different hydrodynamical coefficients used by the model, presented figure 4. The Strouhal number is quite constant at 0.2 for the range of the reduced velocities, which corresponds to the bibliographical results. The evolution of added mass coefficient is classical with a maximum at $V_r = 4.5$ then a decrease until $V_r = 10$. The gap

at $V_r = 10$ comes from the variation of the amplitude of the transverse motion A/D. The mean drag coefficient increases smoothly from 1 to 1.2 with the velocity. The blockage drag coefficient is null for the lowest velocities, then there is a gap for $1.7 < V_r < 2.3$ because oscillations occur in the in-line direction (figure 3) for the *second instability region*. Then this coefficient is increasing during the lock-in for $6 < V_r < 10$ because of the large transverse oscillations and finally decreases smoothly, for $V_r > 10$. The frequency ratio f^*, between the Strouhal frequency f_{st} and the natural frequency in water f_{com} which depends of the added mass variations, shows precisely the origin of the lock-in with a plate at 1 between $V_r = 4.5$ and $V_r = 9.5$ and linear curves before and after the lock-in.

4. CONCLUSION

The behaviour of a single cylinder submit to a current had been modeled by a phenomenological model based on Van Der Pol oscillators. After the presentation of the model and the description of the used parameters, we have compared the model results with some experimental data. The comparison is relatively in good agreement for the mean and standard deviation of the two dimensional cylinder motions. The differences come essentially from the poor set of data for the fluctuating drag coefficient. Some specific experimental tests should be conducted to solve this problem.

Despite those imperfections, an extension will be carried out in order to model wake effects of two cylinders in tandem arrangement. The results will also be compared to experimental data.

5. REFERENCES

Ashino, R. et al, 2000, Behind and Beyond the Matlab ODE Suite. *Computers and Mathematics with Applications* **40**: 491 - 512.

Cantwell, B., Coles, D., 1983, An experimental study of entrainment and transport in the turbulent near wake of a cylinder. *Journal of Fluids Mechanics* **136**: 321 - 374.

Facchinetti, M.L. et al, 2004, Coupling of structure and wake oscillators in vortex-induced vibrations. *Journal of Fluids and Structures* **19**: 123 - 140.

Flemming, D., Williamson, C.H.K., 2005, Vortex-induced vibrations of a pivoted cylinder. *Journal of Fluids Mechanics* **522**: 215 - 252.

Gaurier, B. et al, 2007a, Experimental and numerical results on VIV and WIO. *IUTAM Symposium*. Hamburg, Germany.

Gaurier, B. et al, 2007b, Caractérisation d'effets de sillages rencontrés en mileu offshore. *11ème Journées de l'Hydrodynamique*. Brest, France.

Germain, G. et al, 2006, Vortex and wake effects on closely spaced marine risers. *Flow Induced Vibrations* (PVP ASME). Vancouver, Canada.

Jauvtis, N., Williamson, C.H.K., 2003, Vortex-induced vibration of a cylinder with two degrees of freedom. *Journal of Fluids and Structures* **17**: 1035 - 1042.

Jauvtis, N., Williamson, C.H.K., 2004, The effect of two degrees of freedom on vortex-induced vibration at low mass damping. *Journal of Fluids Mechanics* **509**: 23 - 62.

Kracker, S.C. et al, 1974, Fluctuating lift coefficient for a circular cylinder in cross flow. *Journal of Mechanical Engineering Science* **16**: 215 - 224.

Morison, J.R. et al, 1950, The force exerted by surface waves on piles. Petroleum Transactions. *AIME* **189**: 149 - 154.

Norberg, C., 2001, Flow around a circular cylinder: aspect of fluctuating lift. *Journal of Fluids and Structures* **15**: 459 - 469.

Norberg, C., 2002, Fluctuating lift on a circular cylinder: review and new measurements. *Journal of Fluids and Structures* **17**: 57 - 96.

Sarpkaya, T., 1978, Fluid forces on oscillating cylinders . *Journal of Waterway Port Coastal and Ocean Division ASCE* **104**: 275 - 290.

Sarpkaya, T., 2004, A critical review of the intrinsic nature of vortex-induced vibrations. *Journal of Fluids and Structures* **19**: 389 - 447.

Schlichting, H., 1951, Boundary-Layer Theory. *McGraw-Hill, INC.* Seventh Edition.

Skop, R.A. et al, 1977, Strumming predictions for the Seacon II experimental mooring. *Proc 9th Offshore Techn Conf* **2884**.

Violette, R. et al, 2007, Computation of vortex-induced vibrations of long structures using a wake oscillator model: Comparison with DNS and experiments. *Computers and Structures* **85**: 1134 - 1141.